Field-Induced Hydration Shell Reorganization Enables Electro-osmotic Flow in Nanochannels

Wanqi Zhou, Yufeng Guo, Zhuhua Zhang, Wanlin Guo,* and Hu Qiu†
State Key Laboratory of Mechanics and Control of Mechanical Structures and Key Laboratory for Intelligent Nano Materials and Devices of MOE, Institute of Nano Science, Nanjing University of Aeronautics and Astronautics, Nanjing 210016, China

(Received 21 January 2022; revised 31 October 2022; accepted 17 January 2023; published 21 February 2023)

Electro-osmotic flow is the motion of fluid driven by an applied electric field, for which an electric double layer near a charged surface is deemed essential. Here, we find that electro-osmotic flow can occur in electrically neutral nanochannels in the absence of definable electric double layers through extensive molecular dynamics simulations. An applied electric field is shown to cause an intrinsic channel selectivity between cations and anions, by reorienting the hydration shells of these confined ions. The ion selectivity then results in a net charge density in the channel that induces the unconventional electro-osmotic flow. The flow direction is amenable to manipulation by the field strength and the channel size, which will inform ongoing efforts to develop highly integrated nanofluidic systems capable of complex flow control.

DOI: 10.1103/PhysRevLett.130.084001

When an ionic solution makes contact with a charged surface, an electric double layer (EDL) develops near the surface as a result of the accumulation of oppositely charged counterions. If an external electrical field is applied parallel to the surface, electro-osmotic flow is generated due to the motions of ions in the EDL that drag the rest of the fluid [1,2]. Because of its ability to transport water in miniaturized systems without incorporating any mechanical parts, electro-osmotic flow has found diverse applications in separation [3] and mixing [4], nanopore sensing [5], and micro- and nanofluidic devices [6,7].

Recent progress in fabrication technology has allowed the creation of nanometer-sized channels with various geometries [8–11]. In these nanofluidic systems, the electro-osmotic flow is known to be fundamentally different from those in bulk systems or microchannels [12–17]. Typical examples include anomalous ion distribution near the channel wall [12], electro-osmotic flow in the opposite direction to that predicted by the classical continuum theory [13], and electro-osmotic flow in uncharged channels [16,18,19], etc. These novel electro-osmotic transport phenomena cannot be described directly by EDL-based classical models. The reason is that some physical effects at atomistic length scales (e.g., molecular nature of individual ions and water molecules), negligible in macroscopic systems, are expected to be significant in nanofluidic systems. Nevertheless, many of these transport phenomena can still be rationalized by making corrections to the continuum model [12–14,20,21], as long as the channel dimension is large enough (e.g., > 2.2 nm according to Ref. [12]) to accommodate EDLs. Upon further reduction in the channel dimension, i.e., to the order of the interaction length of the fluid molecules (e.g., sub-2 nm), EDLs have vanished or are strongly overlapped [18,22], which presumably results in breakdown of EDL-based models and necessitates novel electro-osmotic flow mechanisms.

In this Letter, we demonstrate via molecular dynamics (MD) simulations that a steady electro-osmotic flow can develop in electrically neutral, sub-2 nm nanochannels. This electro-osmotic flow is unusual since no definable EDL is present, due to the extremely narrow channel interior and the absence of surface charge on the channel wall. It results from an entirely new mechanism that can be attributed to the presence of a net charge density inside the channels, induced by ion selectivity arising from electric field-induced molecular reorganization in the hydration shells of ions.

The simulation system consists of a 6 nm long carbon nanotube (CNT) embedded between two graphene sheets, attached to a bath of 1 M KCl solution at both ends of the tube (inset of Fig. 1). The CNT channel was chosen as the model system because of its long-recognized potential for nanofluidic applications [20,23–28]. We primarily focused on sub-2 nm CNTs with the diameter d varying from 0.95 to 1.97 nm and also considered wider CNTs to confirm the robustness of our results. An electric field E of 0.05–1 $\mathrm{V\,nm^{-1}}$ was applied parallel to the channel axis to induce the electro-osmotic flow (see Sec. S0 in the Supplemental Material [29] for further simulation details). The field strength adopted here should be experimentally accessible since the fields used in typical nanochannel transport experiments were ranged in 0.000 07–0.44 $\mathrm{V\,nm^{-1}}$ (Fig. S7 in the Supplemental Material [29]).

Figure 1 shows the cumulative flux of water molecules passing through the CNT channels with $d = 1.08$, 1.32,

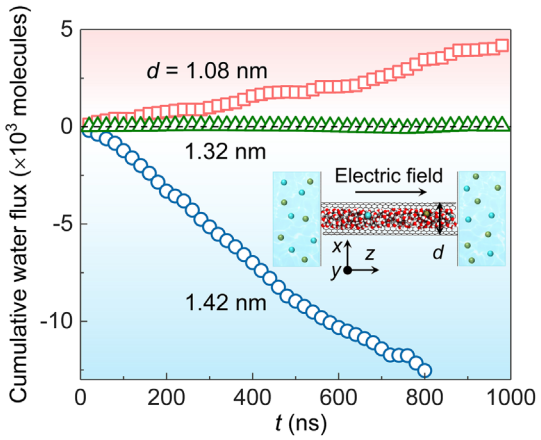

FIG. 1. Cumulative flux of water molecules passing through the channels with diameters of 1.08 (squares), 1.32 (triangles), and 1.42 nm (circles) under an electric field of 0.48 V nm^{-1}. A positive flux means the electro-osmotic flow along $+z$, whereas a negative value corresponds to $-z$. The inset shows the simulation system. A CNT combined with two graphene sheets is placed between two reservoirs filled with KCl solutions. The external electric field is applied parallel to the tube axis (along the $+z$ direction).

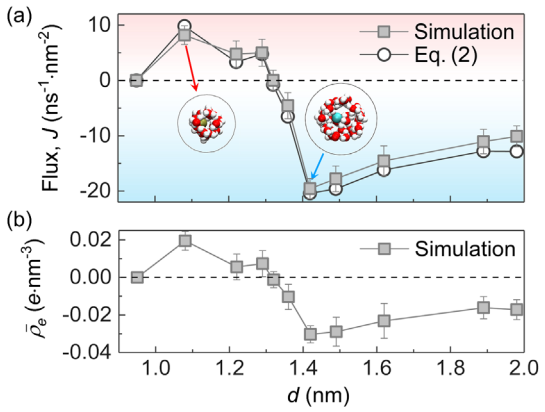

FIG. 2. Water flux J (a) and average net charge density $\bar{\rho}_e$ (b) in nanochannels with different diameters d under an electric field of 0.48 V nm^{-1}. Results in (a) computed using Eq. (2), based on $\bar{\rho}_e$ in (b), are also shown (open circles). Error bars represent standard deviations of five independent simulations (Fig. S8 [29]).

and 1.42 nm, under $E = 0.48$ V nm^{-1}. The cumulative flux at each moment is defined as the difference between the number of water molecules moving in the $+z$ direction (left to right) and that in the contrary. The approximately linear relationship between the flux and simulation time indicates that these systems achieve a steady state of electro-osmotic flow. However, the three CNTs exhibit dramatically different cumulative flux profiles. In the 1.08 nm CNT, the water flux is positive, indicating a steady rightward flow (along the $+z$ direction). For the 1.42 nm CNT, the flux is reversed to be negative, indicating a leftward flow (along the $-z$ direction). Interestingly, no obvious water flux is identified in the CNT with a moderate diameter of 1.32 nm. The observed flow reversal clearly illustrates a crucial role of the channel diameter in determining the direction of the electro-osmotic flow through these electrically neutral, extremely narrow channels.

We further investigated the electro-osmotic flow through all simulated sub-2 nm CNT channels and determined the net water flux J as the slope of the cumulative flux curve (Fig. S8 in the Supplemental Material [29]) divided by the effective area of the channel's cross section, as shown in Fig. 2(a). In the considered narrowest CNT ($d = 0.95$ nm), no net water flux is observed, a consequence of the complete ion rejection of this channel as reported previously [68,83]. As d gradually increases, the electro-osmotic flow develops first along the $+z$ direction when $d < 1.32$ nm, vanishes at $d = 1.32$ nm, and then reverses to the $-z$ direction for $d > 1.32$ nm [Fig. 2(a)], a phenomenon that we term d-dependent reversal of electro-osmotic flow. Clearly, this phenomenon in electrically neutral channels cannot be understood directly using classical continuum models. We note that the existence of EDLs and/or electric field-driven water flow in neutral channels have been reported in previous studies [16,18,19,84], which, in most cases, were attributed to different adsorption affinities of cations and anions onto channel surfaces [16,18,19]. Yet, this mechanism alone cannot account for the observed d-dependent flow reversal, because all CNT channels in the present Letter possess almost identical surface properties (i.e., insensitive to d). In addition, as expected [18,22], the EDLs in our sub-2 nm nanochannels are not as explicit as those in much wider channels, but rather, have vanished or are strongly overlapped (Fig. S9 in the Supplemental Material [29]).

It is known that a nonzero net charge density in the EDL is a prerequisite to yielding the driving force for conventional electro-osmotic flow (e.g., those in microchannels) [22,85,86]. Accordingly, we traced the instantaneous net charge density ρ_e inside the present nanochannels, which can be related to the number of K^+ (n_+) and Cl^- (n_-) by $\rho_e = (n_+ - n_-)e/V_{\text{eff}}$, where e is the elementary charge and V_{eff} is the channel's effective volume. It is rather not surprising that the instantaneous water velocity v shows near-perfect correlation with ρ_e (Fig. S10 [29]). Specifically, a positive (or negative) ρ_e corresponds to a water velocity along the $+z$ (or $-z$) direction, and vice versa. Meanwhile, the average net charge density $\bar{\rho}_e$, determined by averaging ρ_e over the entire MD trajectory, is found to vary in sync with J, as d changes [Fig. 2(b)].

Our additional simulations showed that the presence of the reported electro-osmotic flow is robust against using other simulation systems or parameters, such as the use of a NaCl solution (Fig. S11), different water models (Fig. S12), different Lennard-Jones parameters for carbon atoms (Fig. S13), different channel geometries or wall materials

(Fig. S14), as well as different choices of common simulation protocols (Sec. S1 [29]).

We now turn to understand the relationship between J and $\bar{\rho}_e$ from a theoretical perspective. By applying an external electric field E, the whole aqueous solution in nanochannels feels a body force $F_E = \bar{\rho}_e V_{\text{eff}} E$, acting as the electric driving force. V_{eff} is given by $V_{\text{eff}} = \pi(d_{\text{eff}}/2)^2 l$, with l the channel length and $d_{\text{eff}} = d - \sigma$ the channel's effective diameter (where σ is the van der Waals diameter of wall atoms at ~0.34 nm). Once a steady electro-osmotic flow is achieved, the driving force should be balanced by the fluid-solid friction force F_f, that is, $F_E = F_f$ (as sketched in Fig. S15 [29]). F_f is given by $F_f = \xi A_{\text{wall}} v_s$ [56,87,88], where ξ is the fluid-solid friction coefficient (1.0×10^6 N s m^{-3}, detailed in Sec. S2 of the Supplemental Material [29]), v_s is the slip velocity, and $A_{\text{wall}} = \pi d_{\text{eff}} l$ is the effective contact area between fluid and solid. As the velocity profiles of water flow in CNTs are pluglike [56,89,90], we set v_s equal to the average velocity $\bar{v}$. Altogether, this allows us to express $\bar{v}$ as

$$\bar{v} = \frac{E}{4\xi} d_{\text{eff}} \bar{\rho}_e. \tag{1}$$

Since J is related to $\bar{v}$ according to $J = \bar{v} n_w$, with n_w the density of water (33.5 nm^{-3}), this leads to the relation

$$J = \frac{n_w E}{4\xi} d_{\text{eff}} \bar{\rho}_e. \tag{2}$$

Based on $\bar{\rho}_e$ determined from MD trajectories [Fig. 2(b)], Eq. (2) reproduces well the water flux for all simulated sub-2 nm channels [Fig. 2(a)]. For Eq. (2), it is also worthy to note that J is independent of the channel length l, which again agrees with simulations (Fig. S16 [29]).

Our above results have identified the net charge density inside nanochannels as the decisive factor that accounts for the electro-osmotic flow. The presence of a net charge density manifests as unequal numbers of K^+ and Cl^- ions in the channel, which roots in the nanochannel selectivity between K^+ and Cl^-. For instance, a positive $\bar{\rho}_e$ means that the channel preferentially selects K^+ relative to Cl^-, and vice versa. A reasonable description of the ion selectivity can be provided by comparing the free energy difference between the permeation of K^+ and Cl^-. Figure 3(a) shows the free energy profiles for the systems with 1.08, 1.32, and 1.42 nm CNTs, calculated with the free energy perturbation method (see Sec. S3 for detailed procedures [29]). In the absence of electric fields, the higher energy barriers for moving Cl^- than those for moving K^+ into the CNTs [open symbols in Fig. 3(a)] show that all these nanochannels tend to selectively conduct K^+ ions. This unified intrinsic selectivity of K^+ over Cl^- has also been reported in previous simulations [68,91] and experiments [92], but fails to explain the dramatically different $\bar{\rho}_e$ (and also J) for these three channels (which are positive, zero, and negative in the 1.08, 1.32, and 1.42 nm channels, respectively, according to Fig. 2).

When the effect of electric fields on the system is taken into account, two striking features arise in the free energy profiles [filled symbols in Fig. 3(a)]. First, the free energy barriers increase steeply, regardless of the ion polarity and channel diameter. The barrier increase is validated by several attempts, such as computations with the umbrella sampling method and a demonstration of ion rejection under ultrastrong hydrostatic pressures (Sec. S3 [29]). The second observation related to the external field is the

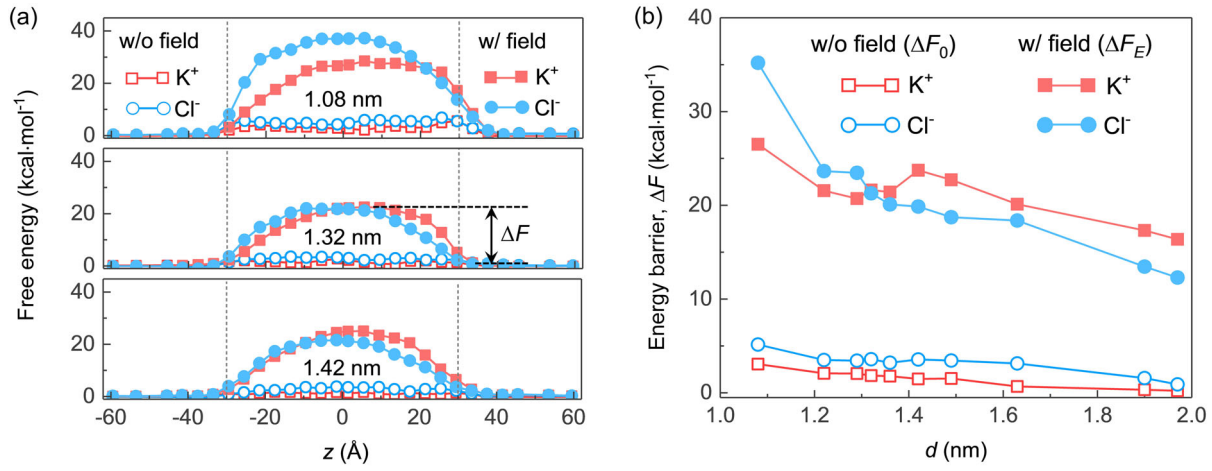

FIG. 3. Free energy profiles of ion permeation through nanochannels. (a) Free energy profiles along the channel axis for K^+ (red) and Cl^- (blue) ions at $d = 1.08$ (top), 1.32 (middle), and 1.42 nm (bottom). The filled and open symbols show the data gained with and without the electric field (0.48 V nm^{-1}), respectively. The vertical dotted lines indicate the positions of the entrance and exit of the channels. (b) Free energy barriers ΔF for K^+ and Cl^- as a function of d, without (open) or with (filled) the electric field. ΔF is defined as the peak height of free energy profiles [see the middle panel in (a)].

reversal in the selectivity between K^+ and Cl^- in some nanochannels. In the 1.08 nm CNT, the barrier of Cl^- remains higher than that of K^+ [top panel in Fig. 3(a)], maintaining its intrinsic K^+ selectivity and resulting in the positive $\bar{\rho}_e$ and thus the electro-osmotic flow along the $+z$ direction (see Figs. 1 and 2). In the 1.42 nm CNT, however, the barrier of Cl^- becomes slightly lower than that of K^+ [bottom panel in Fig. 3(a)], indicating a transition to the Cl^- selectivity from the intrinsic K^+ selectivity in the field-free case. This is consistent with the negative $\bar{\rho}_e$ and the incurred reversed electro-osmotic flow. Finally, in the CNT with a moderate diameter of 1.32 nm, the nearly identical energy barriers between K^+ and Cl^- [middle panel in Fig. 3(a)] are in line with the vanishing $\bar{\rho}_e$ and the absence of electro-osmotic flow in this channel.

We collect in Fig. 3(b) energy barriers (ΔF) for K^+ and Cl^- permeation through the simulated ten sub-2 nm nanochannels, with the corresponding free energy profiles provided in Fig. 3(a) and Fig. S17 [29]. It is found that all the channels with $d > 1.32$ nm become Cl^- selective as an electric field is applied to the system (from K^+ selective in the field-free case), whereas those with $d < 1.32$ nm remain K^+ selective. This trend agrees well with the trend of J or $\bar{\rho}_e$ with respect to d (see Fig. 2).

To understand why the presence of an electric field abruptly increases the energy barrier for ion permeation and leads to the observed d-dependent flow reversal, we carefully examined the electric field-induced change of ion solvation properties inside the nanochannels, such as ion-oxygen radial distribution functions [Fig. S18(a) [29]]. Partial dehydration is a known determinant of the energy barrier for ion permeation through a nanochannel [68,93,94]. In our systems, however, the barrier increase is not caused by the dehydration, because the ion coordination number remains almost unchanged when an electric field is applied [Fig. S18(b) [29]]. It is also known that electric fields can affect water orientation inside the hydration shells [95,96], and we will show below that such field-induced reorientation is responsible for the observed barrier change. The orientation angle θ of a water molecule within an ion's first hydration shell is defined as the angle between its dipole and the line joining the ion to the nearest water atom (being oxygen for K^+ and hydrogen for Cl^-), as sketched in Fig. 4(a). When an electric field is applied, these water molecules experience a significant reorientation, as indicated by a broadening in the θ distribution profiles (Fig. S19 [29]). Such water reorientation should not be a numerical artefact caused by the use of non-polarizable water models, because a similar trend was also observed in *ab initio* MD simulations (Fig. S20 [29]). Furthermore, the reorientation was shown to be robust against using other algorithms for treating the long-range electrostatic interactions in MD simulations (Sec. S1 [29]).

To further quantify the field-induced water reorientation, we calculated the hydration factor f for K^+ (or Cl^-) in all considered situations, defined as the proportion of water having θ values in the range from 136° to 180° (or 37° to 60°) in the first hydration shells [97]. Figure 4(b) shows the hydration factor difference ($f_E - f_0$) and the free energy barrier increase ($\Delta F_E - \Delta F_0$) for different systems induced by the applied field (where the subscripts E and 0 denote the values determined with and without the electric field, respectively). In general, an anticorrelation is found between the ($f_E - f_0$) and ($\Delta F_E - \Delta F_0$) curves for both K^+ and Cl^- in most channels; that is, a decrease in ($f_E - f_0$) corresponds to an increase in ($\Delta F_E - \Delta F_0$), and vice versa. The sole exception found for Cl^- in the 1.08 nm CNT is likely due to the strong confinement that has significantly reoriented its hydration shell in the field-free case [with respect to Cl^- in the bulk solution,

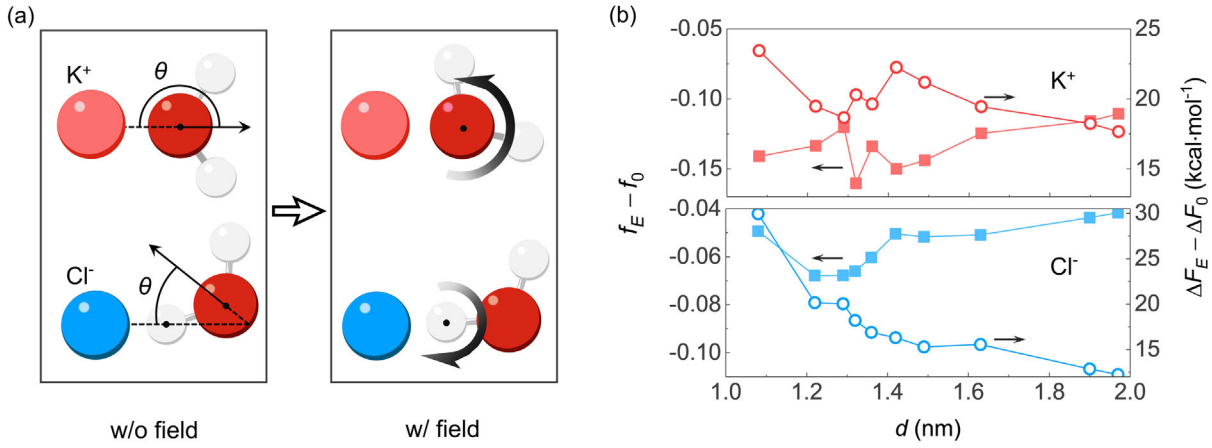

FIG. 4. Ion selectivity mechanisms that result in the electro-osmotic flow. (a) Schematic of the field-induced reorientation of water dipoles in the first hydration shells of K^+ and Cl^-. (b) Hydration factor difference $f_E - f_0$ and free energy barrier increase $\Delta F_E - \Delta F_0$ for K^+ (top) and Cl^- (bottom) against the channel diameter d. The subscripts E and 0 in each variable denote the situation with and without the electric field (0.48 V nm^{-1}), respectively.

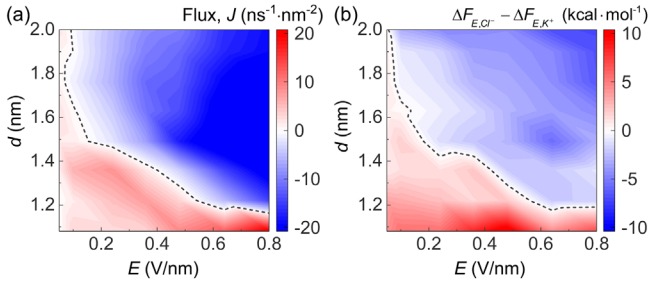

FIG. 5. Water flux (a) and free energy barrier difference between Cl^- and K^+ (b) as a function of channel diameter and electric field strength. The black dashed lines represent vanishing flux (a) or energy barrier difference (b).

see Fig. S19(b)]. These results provide direct evidence that the drastic change in energy barriers originates from electric field-induced reorientation of the first hydration shells of confined ions.

We then examined the influence of the field strength E on the electro-osmotic flow through different channels and plotted the resulting flux map in Fig. 5(a). The threshold diameter for the flow reversal is found to decrease with increasing E (dashed line). Meanwhile, the map of energy barrier difference between Cl^- and K^+ [Fig. 5(b)] displays a similar distribution with the flux map. These results confirm that the field-induced ion selectivity is responsible for the observed electro-osmotic flow.

We also explored the electro-osmotic flow through wider nanochannels with d in the range from 2.17 to 7.44 nm. The simulation results in Fig. S21 [29] show that both J and $\bar{\rho}_e$ are saturated when $d \geq 5.42$ nm, in line with the overlapped θ distribution profiles for the hydration shells of ions inside these channels [98]. Finally, we demonstrated a potential utility of the electro-osmotic flow, by showing that it could be used for separating electrically neutral biomolecules of different sizes (Fig. S22 [29]). It may also find applications in mixing and nanopore sensing, etc., as is the case with usual electro-osmotic flow.

In summary, we find an unconventional electro-osmotic flow phenomenon in electrically neutral nanochannels by comprehensive MD simulations, in which no definable EDL is available. At a given field strength, the electro-osmotic flow direction coincides with that of the external electric field inside cation-selective channels, but becomes opposite to the field in wider, anion-selective channels. The ion selectivity is brought about by water reorientation in the hydration shells of ions induced by the external electric field. Although the electro-osmotic flow is found based on computational investigations, we believe that its implementation is feasible using current experimental techniques (Sec. S4 [29]).

We are grateful to Professors Min Yi and Yanpeng Liu for discussions. This work was supported by National Natural Science Foundation (NSF) of China (12172170, 11972186, T2293691, 12225205, 12150002, 12261160367), Natural Science Foundation of Jiangsu Province (BK20221476, BK20212008), Six Talent Peaks Project in Jiangsu Province (SWYY-024), National Key Research and Development Program of China (2019YFA0705400), Research Fund of State Key Laboratory of Mechanics and Control of Mechanical Structures (MCMS-I-0422K01), Fundamental Research Funds for the Central Universities (NJ2022002), and the Fund of Prospective Layout of Scientific Research for NUAA (Nanjing University of Aeronautics and Astronautics).

*Corresponding author.
wlguo@nuaa.edu.cn
†Corresponding author.
qiuhu@nuaa.edu.cn

[1] S. Ghosal, Electrophoresis **25**, 214 (2004).
[2] T. M. Squires and S. R. Quake, Rev. Mod. Phys. **77**, 977 (2005).
[3] R. Johann and P. Renaud, Electrophoresis **25**, 3720 (2004).
[4] I. Glasgow, J. Batton, and N. Aubry, Lab Chip **4**, 558 (2004).
[5] Y. Zhang, J. Zhao, W. Si, Y. Kan, Z. Xu, J. Sha, and Y. Chen, Small Methods **4**, 1900893 (2020).
[6] C.-H. Chen and J. G. Santiago, J. Microelectromech. Syst. **11**, 672 (2002).
[7] J.-Y. Miao, Z.-L. Xu, X.-Y. Zhang, N. Wang, Z.-Y. Yang, and P. Sheng, Adv. Mater. **19**, 4234 (2007).
[8] T. Mouterde, A. Keerthi, A. Poggioli, S. A. Dar, A. Siria, A. K. Geim, L. Bocquet, and B. Radha, Nature (London) **567**, 87 (2019).
[9] N. Kavokine, R. R. Netz, and L. Bocquet, Annu. Rev. Fluid Mech. **53**, 377 (2021).
[10] J. Shen, G. Liu, Y. Han, and W. Jin, Nat. Rev. Mater. **6**, 294 (2021).
[11] N. Kavokine, M.-L. Bocquet, and L. Bocquet, Nature (London) **602**, 84 (2022).
[12] R. Qiao and N. R. Aluru, J. Chem. Phys. **118**, 4692 (2003).
[13] R. Qiao and N. R. Aluru, Phys. Rev. Lett. **92**, 198301 (2004).
[14] Y. Chen, Z. Ni, G. Wang, D. Xu, and D. Li, Nano Lett. **8**, 42 (2008).
[15] R. B. Schoch, J. Han, and P. Renaud, Rev. Mod. Phys. **80**, 839 (2008).
[16] D. Kim and E. Darve, J. Colloid Interface Sci. **330**, 194 (2009).
[17] L. Vuković, E. Vokac, and P. Král, J. Phys. Chem. Lett. **5**, 2131 (2014).
[18] S. Joseph and N. R. Aluru, Langmuir **22**, 9041 (2006).
[19] A. Dukhin, S. Dukhin, and P. Goetz, Langmuir **21**, 9990 (2005).
[20] R. Qiao and N. R. Aluru, Nano Lett. **3**, 1013 (2003).
[21] W. Zhu, S. J. Singer, Z. Zheng, and A. T. Conlisk, Phys. Rev. E **71**, 041501 (2005).
[22] W. Qu and D. Li, J. Colloid Interface Sci. **224**, 397 (2000).
[23] S. A. Miller, V. Y. Young, and C. R. Martin, J. Am. Chem. Soc. **123**, 12335 (2001).

[24] X. Gong, J. Li, H. Zhang, R. Wan, H. Lu, S. Wang, and H. Fang, Phys. Rev. Lett. **101**, 257801 (2008).

[25] J. Geng, K. Kim, J. Zhang, A. Escalada, R. Tunuguntla, L. R. Comolli, F. I. Allen, A. V. Shnyrova, K. R. Cho, D. Munoz *et al.*, Nature (London) **514**, 612 (2014).

[26] M. Ma, F. Grey, L. Shen, M. Urbakh, S. Wu, J. Z. Liu, Y. Liu, and Q. Zheng, Nat. Nanotechnol. **10**, 692 (2015).

[27] E. Secchi, S. Marbach, A. Niguès, D. Stein, A. Siria, and L. Bocquet, Nature (London) **537**, 210 (2016).

[28] Y.-C. Yao, A. Taqieddin, M. A. Alibakhshi, M. Wanunu, N. R. Aluru, and A. Noy, ACS Nano **13**, 12851 (2019).

[29] See Supplemental Material at http://link.aps.org/supplemental/10.1103/PhysRevLett.130.084001 for methods, influence of the choice of simulation protocols on electro-osmotic flow, calculation of the fluid-solid friction coefficient, calculation and validation of free energy profiles, possible experimental validation of the present findings, and supplemental Figs. S1–S22 and Tables S1 and S2, which includes Refs. [20,28,30–82].

[30] J. C. Phillips, R. Braun, W. Wang, J. Gumbart, E. Tajkhorshid, E. Villa, C. Chipot, R. D. Skeel, L. Kalé, and K. Schulten, J. Comput. Chem. **26**, 1781 (2005).

[31] K. Hart, N. Foloppe, C. M. Baker, E. J. Denning, L. Nilsson, and A. D. Jr. MacKerell, J. Chem. Theory Comput. **8**, 348 (2012).

[32] W. L. Jorgensen, J. Chandrasekhar, J. D. Madura, R. W. Impey, and M. L. Klein, J. Chem. Phys. **79**, 926 (1983).

[33] K. Lindorff-Larsen, S. Piana, K. Palmo, P. Maragakis, J. L. Klepeis, R. O. Dror, and D. E. Shaw, Proteins **78**, 1950 (2010).

[34] H. J. C. Berendsen, J. R. Grigera, and T. P. Straatsma, J. Phys. Chem. **91**, 6269 (1987).

[35] H. W. Horn, W. C. Swope, J. W. Pitera, J. D. Madura, T. J. Dick, G. L. Hura, and T. Head-Gordon, J. Chem. Phys. **120**, 9665 (2004).

[36] U. Essmann, L. Perera, M. L. Berkowitz, T. Darden, H. Lee, and L. G. Pedersen, J. Chem. Phys. **103**, 8577 (1995).

[37] S. E. Feller, Y. Zhang, R. W. Pastor, and B. R. Brooks, J. Chem. Phys. **103**, 4613 (1995).

[38] J. Gumbart, F. Khalili-Araghi, M. Sotomayor, and B. Roux, Biochim. Biophys. Acta **1818**, 294 (2012).

[39] A. Aksimentiev and K. Schulten, Biophys. J. **88**, 3745 (2005).

[40] W. Humphrey, A. Dalke, and K. Schulten, J. Mol. Graphics **14**, 33 (1996).

[41] P. E. Lopes, J. Huang, J. Shim, Y. Luo, H. Li, B. Roux, and A. D. MacKerell Jr, J. Chem. Theory Comput. **9**, 5430 (2013).

[42] H. Yu, T. W. Whitfield, E. Harder, G. Lamoureux, I. Vorobyov, V. M. Anisimov, A. D. MacKerell Jr, and B. Roux, J. Chem. Theory Comput. **6**, 774 (2010).

[43] G. Lamoureux, E. Harder, I. V. Vorobyov, B. Roux, and A. D. MacKerell Jr, Chem. Phys. Lett. **418**, 245 (2006).

[44] B. Grosjean, C. Pean, A. Siria, L. Bocquet, R. Vuilleumier, and M.-L. Bocquet, J. Phys. Chem. Lett. **7**, 4695 (2016).

[45] J. Wong-Ekkabut, M. S. Miettinen, C. Dias, and M. Karttunen, Nat. Nanotechnol. **5**, 555 (2010).

[46] J. Wong-Ekkabut and M. Karttunen, Biochim. Biophys. Acta **1858**, 2529 (2016).

[47] M. J. Abraham, T. Murtola, R. Schulz, S. Páll, S. J. C., B. Hess, and E. Lindahl, SoftwareX **1–2**, 19 (2015).

[48] G. Bussi, D. Donadio, and M. Parrinello, J. Chem. Phys. **126**, 014101 (2007).

[49] M. Thomas and B. Corry, Microfluid. Nanofluid. **18**, 41 (2015).

[50] H. J. Berendsen, J. v. Postma, W. F. Van Gunsteren, A. DiNola, and J. R. Haak, J. Chem. Phys. **81**, 3684 (1984).

[51] S. Nosé, J. Chem. Phys. **81**, 511 (1984).

[52] W. G. Hoover, Phys. Rev. A **31**, 1695 (1985).

[53] I. G. Tironi, R. Sperb, P. E. Smith, and W. F. van Gunsteren, J. Chem. Phys. **102**, 5451 (1995).

[54] D. Frenkel and B. Smit, *Understanding Molecular Simulation: From Algorithms to Applications* (Elsevier, New York, 2001), Vol. 1.

[55] F. Zhu, E. Tajkhorshid, and K. Schulten, Biophys. J. **83**, 154 (2002).

[56] K. Falk, F. Sedlmeier, L. Joly, R. R. Netz, and L. Bocquet, Nano Lett. **10**, 4067 (2010).

[57] J. A. Thomas and A. J. McGaughey, Nano Lett. **8**, 2788 (2008).

[58] J. A. Thomas and A. J. H. McGaughey, Phys. Rev. Lett. **102**, 184502 (2009).

[59] J. S. Babu and S. P. Sathian, J. Chem. Phys. **134**, 194509 (2011).

[60] L. Wang, R. S. Dumont, and J. M. Dickson, J. Chem. Phys. **137**, 044102 (2012).

[61] S. K. Kannam, B. Todd, J. S. Hansen, and P. J. Daivis, J. Chem. Phys. **138**, 094701 (2013).

[62] T. B. Sisan and S. Lichter, Microfluid. Nanofluid. **11**, 787 (2011).

[63] W. Cai, T. Sun, P. Liu, C. Chipot, and X. Shao, J. Phys. Chem. B **113**, 7836 (2009).

[64] S. B. Dixit and C. Chipot, J. Phys. Chem. A **105**, 9795 (2001).

[65] In Silico Alchemy: A Tutorial for Alchemical Free-energy Perturbation Calculations with NAMD, https://www.ks.uiuc.edu/Training/Tutorials/namd/FEP/tutorial-FEP.pdf.

[66] P. Liu, F. Dehez, W. Cai, and C. Chipot, J. Chem. Theory Comput. **8**, 2606 (2012).

[67] G. Hummer, L. R. Pratt, and A. E. GarcÍa, J. Phys. Chem. **100**, 1206 (1996).

[68] C. Song and B. Corry, J. Phys. Chem. B **113**, 7642 (2009).

[69] B. Roux, Comput. Phys. Commun. **91**, 275 (1995).

[70] S. Kumar, J. M. Rosenberg, D. Bouzida, R. H. Swendsen, and P. A. Kollman, J. Comput. Chem. **13**, 1011 (1992).

[71] J. K. Holt, H. G. Park, Y. Wang, M. Stadermann, A. B. Artyukhin, C. P. Grigoropoulos, A. Noy, and O. Bakajin, Science **312**, 1034 (2006).

[72] I. S. Joung and T. E. Cheatham III, J. Phys. Chem. B **112**, 9020 (2008).

[73] S. Gravelle, L. Joly, F. Detcheverry, C. Ybert, C. Cottin-Bizonne, and L. Bocquet, Proc. Natl. Acad. Sci. U.S.A. **110**, 16367 (2013).

[74] J. A. Wendel and W. A. Goddard III, J. Chem. Phys. **97**, 5048 (1992).

[75] J. P. Perdew, K. Burke, and M. Ernzerhof, Phys. Rev. Lett. **77**, 3865 (1996).

[76] J. VandeVondele, M. Krack, F. Mohamed, M. Parrinello, T. Chassaing, and J. Hutter, Comput. Phys. Commun. **167**, 103 (2005).

[77] G. Lippert, J. Hutter, and M. Parrinello, Mol. Phys. **92**, 477 (1997).
[78] S. Goedecker, M. Teter, and J. Hutter, Phys. Rev. B **54**, 1703 (1996).
[79] C. Hartwigsen, S. Goedecker, and J. Hutter, Phys. Rev. B **58**, 3641 (1998).
[80] S. Grimme, J. Antony, S. Ehrlich, and H. Krieg, J. Chem. Phys. **132**, 154104 (2010).
[81] H. Li, J. S. Francisco, and X. C. Zeng, Proc. Natl. Acad. Sci. U.S.A. **112**, 10851 (2015).
[82] P. Umari and A. Pasquarello, Phys. Rev. Lett. **89**, 157602 (2002).
[83] B. Corry, J. Phys. Chem. B **112**, 1427 (2008).
[84] S. Salman, Y. Zhao, X. Zhang, and J. Su, J. Chem. Phys. **153**, 184503 (2020).
[85] S. Levine, J. Marriott, G. Neale, and N. Epstein, J. Colloid Interface Sci. **52**, 136 (1975).
[86] R. J. Hunter, *Zeta Potential in Colloid Science* (Academic Press, New York, 1981).
[87] W. Xiong, J. Z. Liu, M. Ma, Z. Xu, J. Sheridan, and Q. Zheng, Phys. Rev. E **84**, 056329 (2011).
[88] C. Wang, B. Wen, Y. Tu, R. Wan, and H. Fang, J. Phys. Chem. C **119**, 11679 (2015).
[89] S. Joseph and N. R. Aluru, Nano Lett. **8**, 452 (2008).
[90] K. Falk, F. Sedlmeier, L. Joly, R. R. Netz, and L. Bocquet, Langmuir **28**, 14261 (2012).
[91] M. Thomas and B. Corry, Phil. Trans. R. Soc. A **374**, 20150020 (2016).
[92] F. Fornasiero, H. G. Park, J. K. Holt, M. Stadermann, C. P. Grigoropoulos, A. Noy, and O. Bakajin, Proc. Natl. Acad. Sci. U.S.A. **105**, 17250 (2008).
[93] M. Zwolak, J. Lagerqvist, and M. Di Ventra, Phys. Rev. Lett. **103**, 128102 (2009).
[94] S. Sahu, M. Di Ventra, and M. Zwolak, Nano Lett. **17**, 4719 (2017).
[95] Z. He, H. Cui, S. Hao, L. Wang, and J. Zhou, J. Phys. Chem. B **122**, 5991 (2018).
[96] X. Wu, L. Lu, Y. Zhu, Y. Zhang, W. Cao, and X. Lu, Fluid Phase Equilib. **353**, 1 (2013).
[97] Q. Shao, J. Zhou, L. Lu, X. Lu, Y. Zhu, and S. Jiang, Nano Lett. **9**, 989 (2009).
[98] Equation (2) is not strictly applicable in these wide channels, because the charge density away from the channel surface may differ significantly from that near the surface in wide channels and such inhomogeneous charge distribution was not considered when deriving Eq. (2).